







Article

New Cyclopiane Diterpenes and Polyketide Derivatives from Marine Sediment-Derived Fungus *Penicillium antarcticum* KMM 4670 and Their Biological Activities

Anton N. Yurchenko ^{1,*}, Olesya I. Zhuravleva ^{1,2}, Olga O. Khmel ², Galina K. Oleynikova ¹, Alexandr S. Antonov ¹, Natalya N. Kirichuk ¹, Viktoria E. Chausova ¹, Anatoly I. Kalinovsky ¹, Dmitry V. Berdyshev ¹, Natalya Y. Kim ¹, Roman S. Popov ¹, Ekaterina A. Chingizova ¹, Artur R. Chingizov ¹, Marina P. Isaeva ¹ and Ekaterina A. Yurchenko ^{1,*}

¹ G.B. Elyakov Pacific Institute of Bioorganic Chemistry, Far Eastern Branch of the Russian Academy of Sciences, Prospect 100-Letiya Vladivostoka, 159, Russky Island, Vladivostok 690022, Russia; zhuravleva.oi@dvfu.ru (O.I.Z.); antonov_as@piboc.dvo.ru (A.S.A.); sheflera@bk.ru (N.N.K.); v.chausova@gmail.com (V.E.C.); kaaniv@piboc.dvo.ru (A.I.K.); berdyshev@piboc.dvo.ru (D.V.B.); kim_ny@piboc.dvo.ru (N.Y.K.); popov_rs@piboc.dvo.ru (R.S.P.); martyyas@mail.ru (E.A.C.); chingizov_ar@piboc.dvo.ru (A.R.C.); issaeva@piboc.dvo.ru (M.P.I.)

² Institute of High Technologies and Advanced Materials, Far Eastern Federal University, 10 Ajax Bay, Russky Island, Vladivostok 690922, Russia; khmel.oo@dvfu.ru

* Correspondence: yurchenkoan@piboc.dvo.ru (A.N.Y.); eyurch@piboc.dvo.ru (E.A.Y.)

Abstract: Two new cyclopiane diterpenes and a new cladosporin precursor, together with four known related compounds, were isolated from the marine sediment-derived fungus *Penicillium antarcticum* KMM 4670, which was re-identified based on phylogenetic inference from ITS, *BenA*, *CaM*, and *RPB2* gene regions. The absolute stereostructures of the isolated cyclopienes were determined using modified Mosher's method and quantum chemical calculations of the ECD spectra. The isolation from the natural source of two biosynthetic precursors of cladosporin from a natural source has been reported for the first time. The antimicrobial activities of the isolated compounds against *Staphylococcus aureus*, *Escherichia coli*, and *Candida albicans* as well as the inhibition of staphylococcal sortase A activity were investigated. Moreover, the cytotoxicity of the compounds to mammalian cardiomyocytes H9c2 was studied. As a result, new cyclopiane diterpene 13-*epi*-conidiogenone F was found to be a sortase A inhibitor and a promising anti-staphylococcal agent.

Keywords: *Penicillium antarcticum*; phylogeny; re-identification; cyclopienes; polyketides; antimicrobial activity; sortase A; cytotoxicity



Citation: Yurchenko, A.N.; Zhuravleva, O.I.; Khmel, O.O.; Oleynikova, G.K.; Antonov, A.S.; Kirichuk, N.N.; Chausova, V.E.; Kalinovsky, A.I.; Berdyshev, D.V.; Kim, N.Y.; et al. New Cyclopiane Diterpenes and Polyketide Derivatives from Marine Sediment-Derived Fungus *Penicillium antarcticum* KMM 4670 and Their Biological Activities. *Mar. Drugs* **2023**, *21*, 584. <https://doi.org/10.3390/md21110584>

Academic Editor: Jie Bao

Received: 10 October 2023

Revised: 7 November 2023

Accepted: 7 November 2023

Published: 9 November 2023



Copyright: © 2023 by the authors. Licensee MDPI, Basel, Switzerland. This article is an open access article distributed under the terms and conditions of the Creative Commons Attribution (CC BY) license (<https://creativecommons.org/licenses/by/4.0/>).

1. Introduction

Marine fungi are a significant source of compounds with antimicrobial properties [1], among which sediment-derived fungi can be one of the promising sources of novel secondary metabolites [2].

The section *Canescentia* of the genus *Penicillium*, besides species *P. canescens* and *P. janczewskii*, includes such widespread species as *P. antarcticum*, *P. atrovenetum*, and *P. novae-zeelandiae* which are predominantly isolated from soil and leaf litter [3]. Difficulties in using morphological characters to identify strains make identification of this group continually problematic and induce a re-evaluation using phylogenetic data. Earlier *Penicillium attenuatum* KMM 4671, *P. ochotense* KMM 4670, and *P. piltunense* KMM 4668 were isolated from the Sea of Okhotsk and reported as new species [3], but recently Visagie and co-authors reduced these fungi to synonymy with *P. antarcticum* from series *Atroveneta* [4]. The assumption about several frameshift mutations in coding regions at sequence ends, which may imply low-quality sequence reads, needs to be verified.

Recently, seven fungal strains belonging to the *Atroveneta* series were investigated, and one or more species produced asperentins (2/7 species), atlantinones and rastins (4/7 species), patulin (3/7 species), atrovenetins (2/7 species), antarones (1/7 species), auranti-amine (1/7 species), benzomalvins (1/7 species), fischerin (1/7 species), and haenamindole (1/7 species) [4]. Various strains of *P. antarcticum* were described as producers of simple diketopiperazines *cis*-cyclo(4*R*-Hyp, *L*-Leu), *trans*-cyclo(4*R*-Hyp, *L*-Leu), *cis*-cyclo(4*R*-Hyp, *L*-Phe), cyclo-(*L*-Pro, Gly) [5], cladosporin (=asperentin) and its varied derivatives [6–8], antarones A and B [9], alkaloids aurantioclavine and chrysogine [6,7], itaconic acid and its derivatives [5], patulin, terrestric and violaceic acids [6,7], *cis*-4-hydroxymellein [5], and andrastin-type meroterpenoids [10]. Moreover, new carotane sesquiterpenoids piltunines A–F as well as known penigrisacid D were isolated from the fungus *Penicillium piltunense* KMM 4668 [11], which recently was suggested to be *P. antarcticum* [4]. Thus, *P. antarcticum* strains are rich sources of mainly structurally diverse polyketides, including well-known bioactive cladosporin.

Cladosporin was first isolated as an antifungal secondary metabolite from the endophytic fungus *Cladosporium cladosporioides* [12]. Later, its specific antimalarial activity-targeted *Plasmodium falciparum* cytosolic lysyl-tRNA synthetase was found [13]. Aminoacyl-tRNA synthetases (aaRSs) activate specific amino acids and attach them to tRNAs, which participate in the translation of messenger RNAs and synthesis of proteins at the ribosome. These enzymes are pivotal for protein biosynthesis and seminal targets for drug discovery and design. Currently, the IleRS inhibitor mupirocin and the LeuRS inhibitor tavaborole are cases of the successful clinical viability of aaRS inhibitors [14]. Despite the high activity and specificity against *Plasmodium falciparum* as well as its antibacterial, antifungal, and herbicidal effects [15,16], cladosporin has a high clearance rate in the body and poor oral bioavailability in an in vivo assay [17]; therefore, it has never been put on the market as a drug. The search for cladosporin derivatives with better pharmacological properties is advisable, and some results have already been obtained [18]. Moreover, a study of secondary metabolites from cladosporin-producing fungi may result in the isolation of new antibiotics.

In the current study, we re-identified the fungal strain KMM 4670, isolated its secondary metabolites, and elucidated the structures of the obtained compounds. Moreover, the antimicrobial activity of isolated compounds against *Staphylococcus aureus*, *Escherichia coli*, and *Candida albicans* as well as its influence on sortase A activity were evaluated.

2. Results

2.1. Molecular Re-Identification of the Fungal Strain

In this study, to clarify the taxonomic position of the strain KMM 4670, we re-sequenced the molecular markers, such as ITS and partial *BenA* and *CaM* regions, and additionally sequenced the *RPB2* region. Approximately 580 bp fragments of the ITS region, about 500 bp fragments of the partial *BenA* and *CaM* regions, and 730 bp fragments of the partial *RPB2* gene were successfully amplified. A BLAST search showed that the partial *CaM* and *RPB2* gene sequences were 100% identical with the sequences of the ex-type strain *Penicillium antarcticum* CBS 100492, while the ITS and partial *BenA* regions were more than 99% identical. The phylogenetic ML tree of the concatenated ITS–*BenA*–*CaM*–*RPB2* gene sequences clearly showed that the strain KMM 4670 is clustered with the ex-type strain *P. antarcticum* CBS 100492 (Figure 1).

Thus, the new thorough investigation confirmed earlier conclusions that the strain KMM 4670 should be identified as *Penicillium antarcticum*.

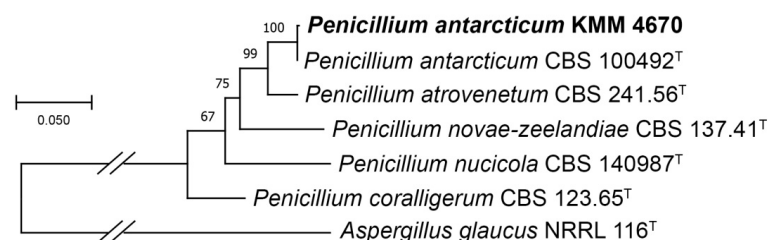


Figure 1. ML tree based on concatenated ITS–BenA–CaM–RPB2 nucleotide sequences showing the phylogenetic position of the strain KMM 4670 among members of genus *Penicillium* section *Canescentia*, series *Atroveneta*. Bootstrap values (%) of 1000 replications. The scale bars represent 0.05 substitutions per site.

2.2. Isolated Compounds

From *P. antarcticum* KMM 4670, new cyclopiane diterpenes 4-hydroxyleptosphin C; (1), 13-*epi*-conidiogenone F (2), and new pentaketide derivative antaketide A (5) as well as known conidiogenone F (3) [19,20], leptosphin C; (4) [21], 2-((2*R*,6*S*)-6-methyltetrahydro-2*H*-pyran-2-yl)acetic acid (6) [22], and cladosporin (7) [12] were isolated (Figure 2).

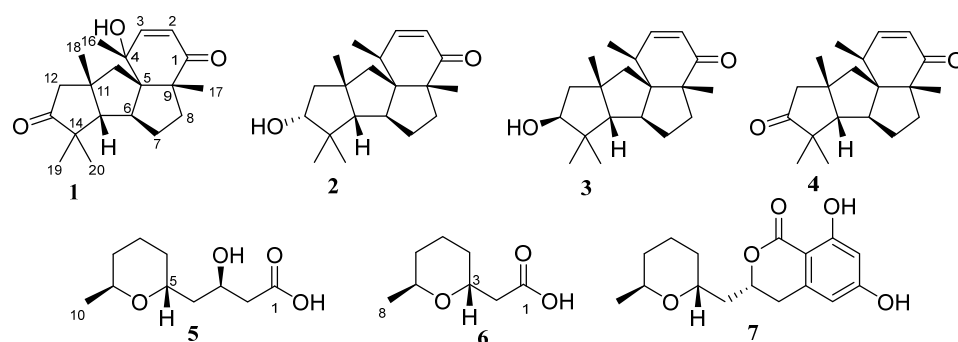


Figure 2. Structures of isolated compounds 1–7.

The molecular formula of **1** was determined as $C_{20}H_{28}O_3$ based on the analysis of the (+)-HRESIMS spectrum (Figure S38) containing the peak of the cationized molecule $[M+Na]^+$ (m/z 339.1933) and was confirmed by the ^{13}C NMR data. The 1H and ^{13}C NMR spectra of compound **1** (Table 1, Figures S1 and S2) revealed the presence of five methyl groups (δ_C 34.3, δ_H 1.41; δ_C 30.1, δ_H 1.11; δ_C 29.1, δ_H 1.41; δ_C 21.7, δ_H 1.08; δ_C 20.6, δ_H 1.21), four sp^3 -methylene groups (δ_C 51.5, δ_H 2.85, 2.33; δ_C 48.8, δ_H 2.27, 1.87; δ_C 40.0, δ_H 2.12, 1.75; δ_C 34.5, δ_H 1.62, 1.23), two sp^3 -methine (δ_C 72.3, δ_H 1.86; δ_C 52.0, δ_H 2.79), and two sp^2 -methine (δ_C 157.0, δ_H 6.68; δ_C 126.1, δ_H 5.86) groups as well as four quaternary sp^3 -carbons (δ_C 65.1, 58.2, 50.7, 44.4), an oxygenated quaternary sp^3 carbon (δ_C 74.2), and two ketones (δ_C 224.9, 205.0).

The COSY correlations (Figure 3 and Figure S6) revealed the spin systems H(15)–H(6)–H(7)–H(8) and H(2)–H(3). The HMBC correlations (Figure 3 and Figure S5) from H-2 (δ_H 6.68) to C-4 (δ_C 74.2) and C-9 (δ_C 58.2); from H-3 (δ_H 5.86) to C-1 (δ_C 205.0), C-5 (δ_C 65.1), C-10 (δ_C 48.8), and C-16 (δ_C 29.1); from H₃-16 (δ_H 1.41) to C-3 (δ_C 157.0), C-4, and C-5; from H₂-8 (δ_H 2.12, 1.75) to C-1, C-7 (δ_C 34.5), and C-9; from H₂-7 (δ_H 1.62, 1.23) to C-6 (δ_C 52.0), C-8 (δ_C 40.0), and C-15 (δ_C 72.3); from H-6 (δ_H 2.79) to C-4, C-5, C-7, C-14 (δ_C 50.7), and C-15; from H-15 (δ_H 1.86) to C-5, C-6, C-7, C-11 (δ_C 44.4), C-12 (δ_C 51.5), C-13 (δ_C 224.9), C-14 (δ_C 50.7), and C-20 (δ_C 30.1); from H₂-10 (δ_H 2.27, 1.87) to C-4, C-5, C-11, and C-12; from H₂-12 (δ_H 2.85, 2.33) to C-10, C-11, C-13, C-15, and C-18 (δ_C 34.3); from H₃-17 (δ_H 1.21) to C-1, C-5, C-8, and C-9; from H₃-18 (δ_H 1.41) to C-10, C-11, C-12, and C-15; and from both H₃-19 (δ_H 1.08) and H₃-20 (δ_H 1.11) to C-13, C-14, and C-15 established a cyclopiane-type core of **1** with keto-groups at C-1 and C-13 and a double bond between C-2 and C-3. A

location of an OH-group at C-4 was suggested based on the downfield chemical shift of C-4 together with the presence of a third oxygen according to the MS data.

Table 1. NMR data (700 MHz, CDCl₃, δ in ppm) for compounds **1** and **2**.

Position	1		2	
	δ_C , Type	δ_H , Mult (J in Hz)	δ_C , Type	δ_H , Mult (J in Hz)
1	205.0, C		206.1, C	
2	126.1, CH	5.86, d (10.2)	127.7, CH	5.97, d (10.0)
3	157.0, CH	6.68, d (10.3)	154.8, CH	6.93, dd (10.0, 5.9)
4	74.2, C		38.3, CH	2.96, m
5	65.1, C		60.5, C	
6	52.0, CH	2.79, dd (9.3, 5.0)	55.1, CH	2.52, m
7	34.5, CH ₂	α : 1.62, m β : 1.23, m	35.1, CH ₂	α : 1.64, m β : 1.19, m
8	40.0, CH ₂	α : 2.12, m β : 1.75, td (13.7, 7.0)	39.8, CH ₂	α : 1.67, m β : 2.08, dd (11.0, 5.3)
9	58.2, C		57.8, C	
10	48.8, CH ₂	α : 2.27, d (15.2) β : 1.87, d (15.0)	47.5, CH ₂	α : 2.03, d (14.7) β : 1.68, d (14.7)
11	44.4, C		48.7, C	
12	51.5, CH ₂	α : 2.85, d (18.8) β : 2.33, d (18.8)	48.5, CH ₂	α : 1.73, dd (13.4, 7.1) β : 1.98, dd (13.4, 6.5)
13	224.9, C		82.8, CH	3.92, t (6.8)
14	50.7, C		45.2, C	
15	72.3, CH	1.86, d (5.1)	73.6, CH	1.51, d (5.3)
16	29.1, CH ₃	1.41, s	19.0, CH ₃	1.16, d (7.1)
17	20.6, CH ₃	1.21, s	21.4, CH ₃	1.21, s
18	34.3, CH ₃	1.41, s	32.1, CH ₃	1.22, s
19	21.7, CH ₃	1.08, s	21.1, CH ₃	0.94, s
20	30.1, CH ₃	1.11, s	31.5, CH ₃	1.05, s

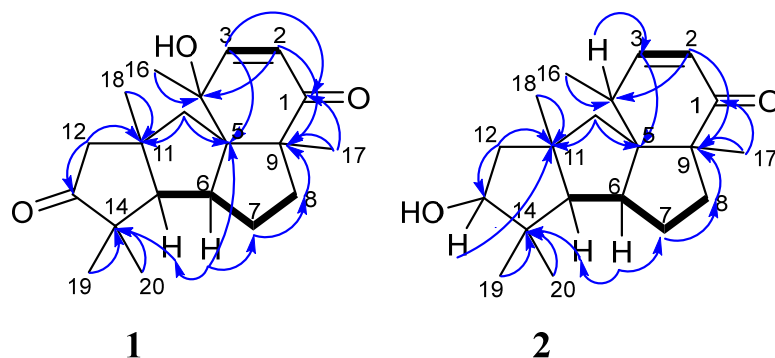


Figure 3. Key HMBC (arrows) and COSY (bold lines) correlations in compounds **1** and **2**.

It should be noted that the structure and NMR data of **1** were very close to known leptosphin C (**4**) [21] with additional hydroxy group at C-4.

The relative stereoconfigurations of **1** were determined using ROESY data (Figures 4 and S7). The ROESY correlations H-12 α /H-10 α ; H-15/H-7 β ; H₃-17/H-10 β ; H₃-18/H-10 β and H-15; H₃-19/H-6; H₃-20/H-12 β ; and H-15 revealed the same relative stereostructure with leptosphin C (**4**) [21] and other members of the cyclopiane group.

The absolute stereostructure of **1** was established as 4*R*,5*S*,6*S*,9*R*,11*S*,15*S* based on the comparison of experimental and calculated ECD spectra (Figure 5). Compound **1** was named 4-hydroxyleptosphin C.

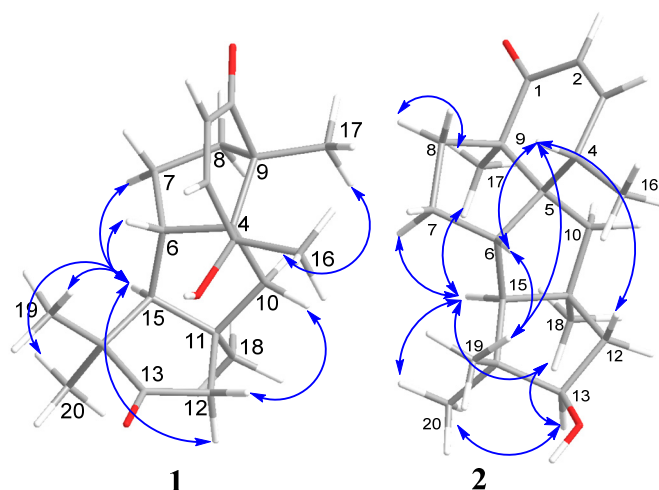


Figure 4. Key ROESY correlations in compounds **1** and **2**.

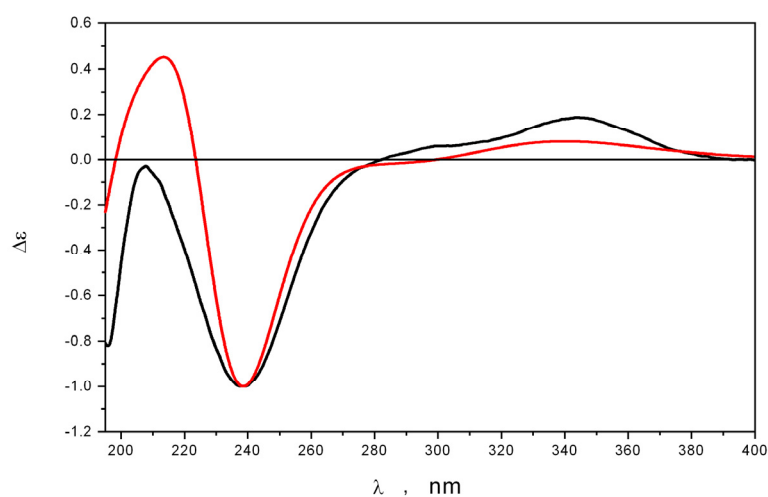


Figure 5. The experimental (black) and calculated (red) ECD spectra of **1**.

The molecular formula of **2** was determined as $C_{20}H_{30}O_2$ based on the (+)-HRESIMS spectrum (Figure S39) containing the peak of the cationized molecule $[M+Na]^+$ (m/z 325.2142) and was confirmed by the ^{13}C NMR data. The main features of 1H and ^{13}C NMR spectra (Table 1, Figures S3 and S4) were close to those of known cyclopiane conidiogenone F (**3**) [19] with significant differences in some signals. The HMBC correlations (Figures 3 and S12) confirmed a planar structure of **2** to be the same as conidiogenone F (**3**).

The ROESY correlations (Figure 4 and Figure S14) H-15 (δ_H 1.51)/H₃-20 (δ_H 1.05), H₃-18 (δ_H 1.22), H₃-17 (δ_H 1.21), and H-7 β (δ_H 1.19); H-13 (δ_H 3.92)/H₃-20 and H₃-18; H-4 (δ_H 2.96)/H₃-19 (δ_H 0.94), H-12 α (δ_H 1.73), and H-6 (δ_H 2.52); H-6/H₃-19; H₃-17/H-8 β (δ_H 2.08); H₃-16 (δ_H 1.16)/H-10 α (δ_H 2.03) and H-10 β (δ_H 1.68); and H₃-18/H-10 β established the relative configurations of all stereocenters, which was the same as those for conidiogenone F (**3**) with the exception of C-13.

The absolute configurations of the chiral centers of **2** could not be determined with a modified Mosher's method [23] due to an insufficient amount of this compound. Therefore, this method was used for compound **3**. The esterification of **3** with (*S*)- and (*R*)-MTPA chloride occurred at the C-13 hydroxy group to yield the (*R*)- and (*S*)-MTPA esters **3a** and **3b**, respectively. The observed chemical shift differences $\Delta\delta(\delta_S-\delta_R)$ (Figures 6 and S45–S48) indicated the 13*S* configuration, and therefore, the absolute configurations other chiral centers of **3** were established as 4*S*,5*S*,6*S*,9*R*,11*S*,15*S*. Due to the identity of relative stereochemistry in the diterpene core, the absolute configurations of **2** were determined as 4*S*,5*S*,6*S*,9*R*,11*S*,13*R*,15*S*. Compound **2** was named 13-*epi*-conidiogenone F.

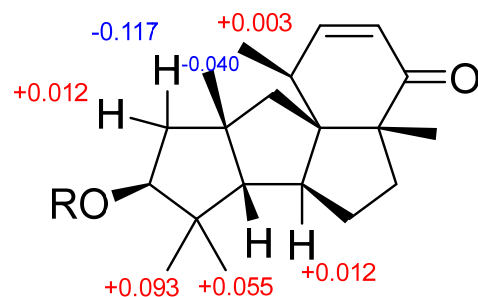


Figure 6. $\Delta\delta(\delta_S-\delta_R)$ values (in ppm) for MTPA esters of **3**.

The absolute configurations of leptosphin C; (**4**) were suggested as 4*S*,5*S*,6*S*,9*R*,11*S*,15*S* based on obvious biogenetic relationships with **1–3**.

The molecular formula of **5** was determined as $C_{10}H_{18}O_4$ based on the (+)-HRESIMS spectrum (Figure S42) containing the peak of the cationized molecule $[M+Na]^+$ (m/z 225.1097) and was confirmed by the ^{13}C NMR data. The 1H and ^{13}C NMR spectra of **5** (Table 2 and Figures S19 and S20) showed the presence of a methyl group (δ_C 18.6, δ_H 1.23), five methylene groups (δ_C 41.2, δ_H 2.57, 2.56; δ_C 39.4, δ_H 1.87, 1.58; δ_C 30.8, δ_H 1.72, 1.37; δ_C 30.7, δ_H 1.62, 1.42; δ_C 18.3, δ_H 1.72, 1.64), three oxygenated methine groups (δ_C 68.3, δ_H 4.05; δ_C 67.8, δ_H 4.08; δ_C 65.9, δ_H 4.29), and a carboxyl group (δ_C 174.9).

Table 2. NMR data (700 MHz, δ in ppm) for compounds **5** and **6**.

Position	5 ^a		6 ^b	
	δ_C , Mult	δ_H (J in Hz)	δ_C , Mult	δ_H (J in Hz)
1	174.9, C		172.5, C	
2	41.2, CH ₂	a: 2.56, brd (5.3) b: 2.57, brd (6.8)	39.1, CH ₂	a: 2.43, dd (14.9, 6.0) b: 2.58, dd (14.9, 7.8)
3	65.9, CH	4.29, m	68.7, CH	4.19, m
4	39.4, CH ₂	a: 1.58, m b: 1.87, ddd (14.4, 9.0, 3.4)	30.3, CH ₂	a: 1.37, m b: 1.67, m
5	67.8, CH	4.08, m	18.9, CH ₂	1.65, m
6	30.6, CH ₂	a: 1.42, m b: 1.62, m	32.2, CH ₂	a: 1.26, m b: 1.64, m
7	18.3, CH ₂	a: 1.64, m b: 1.72, m	67.7 CH	3.90, m
8	30.8, CH ₂	a: 1.37, m b: 1.72, m	20.0, CH ₃	1.12, d (6.4)
9	68.3, CH	4.05, m		
10	18.6, CH ₃	1.23, d (6.5)		

^a CDCl₃; ^b acetone-d₆.

A single spin system H₂(2)–H(3)–H₂(4)–H(5)–H₂(6)–H₂(7)–H₂(8)–H(9)–H₃(10) was elucidated from the COSY correlations (Figure 7 and Figure S24). The HMBC correlations of **5** (Figures 7 and S23) from H₂-2 (δ_H 2.56, 2.57) to C-1 (δ_C 174.9) and C-3 (δ_C 65.9); from H-3 (δ_H 4.29) to C-1; from H-5 (δ_H 4.08) to C-4 (δ_C 39.4), C-6 (δ_C 30.6), and C-9 (δ_C 68.3); and from H-9 (δ_H 4.05) to C-5 (δ_C 67.8), C-8 (δ_C 30.8), and C-10 (δ_C 18.6) make it possible to close the tetrahydropyran ring through oxygen between C-5 and C-9 and add a carboxyl group to methylene C-2.

The NOESY correlations (Figure S25) between H-5 and H₃-10 (δ_H 1.23) revealed the same relative stereostructure of the tetrahydropyran moiety of **5**.

To establish absolute stereo configurations, an attempt was made to apply a modified Mosher's method. Unfortunately, in the preparation of MTPA esters at 3-OH, compound **5** was destroyed. Nevertheless, the absolute configurations of all stereocenters in **5** were suggested based on obvious biogenetic relationships between **5**, **6**, and **7** [17].

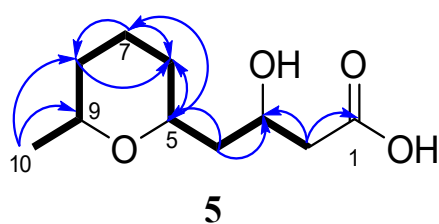


Figure 7. Key HMBC (arrows) and COSY (bold lines) correlations in compound **5**.

To the best of our knowledge, the established structure of compound **5** was new, and this compound was named antaketide A.

2.3. Biological Activity of Isolated Compounds

2.3.1. The Influence on *S. aureus*, *E. coli*, and *C. albicans*

The influence of compounds **1–6** on the growth and biofilm formation of *S. aureus*, *E. coli*, and *C. albicans* was investigated. Cladosporin (**7**) is a naturally occurring fungal metabolite with potent antibacterial, antifungal, insecticidal, and anti-inflammatory activities as well as plant growth regulatory effects [16]. Therefore, its biological activity in the present work was not studied.

The effects of compounds **1–6** on the growth and biofilm formation of Gram-positive bacteria *Staphylococcus aureus* are presented in Figure 8.

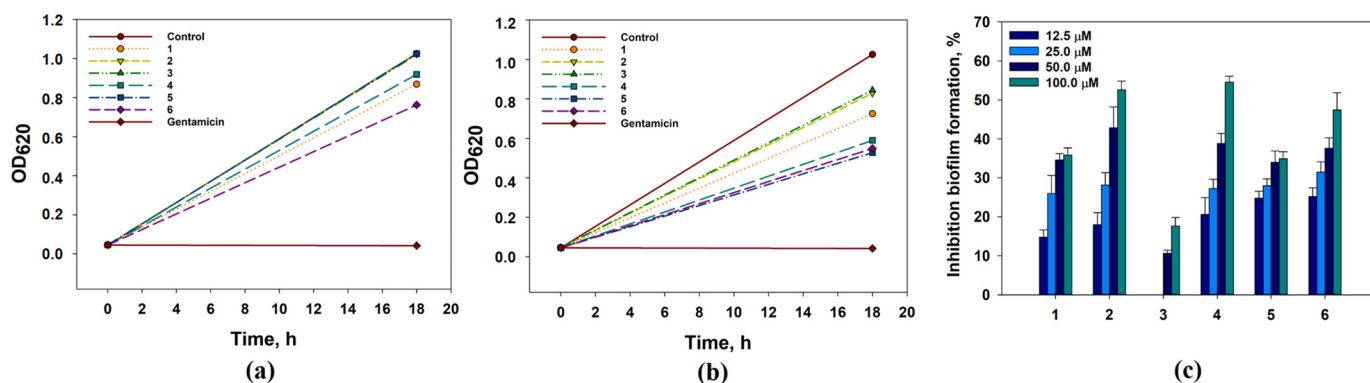


Figure 8. The effect of compounds **1–6** at concentrations of 12.5 µM (a) and 100.0 µM (b) on *Staphylococcus aureus* growth. Gentamicin was used as a positive control at a concentration of 1 mg/mL. (c) The effect of compounds **1–6** on the biofilm formation. The data are presented as a mean \pm standard mean error. All experiments were carried out in independent triplicates.

4-Hydroxyleptosphin C (**1**), at concentrations of 12.5 µM and 100 µM, inhibited *S. aureus* growth by 15.3% and 29.3%, respectively. The prevention of the biofilm formation by 15.9% and 34.5% was observed when the concentrations of **1** were 12.5 µM and 100 µM, respectively.

13-*epi*-conidiogenone F (**2**) showed a weak inhibition of *S. aureus* growth by 19.1% at 100 µM and no effect at 12.5 µM, but this one significantly prevented *S. aureus* biofilm formation from 37.9% at 12.5 µM to 52.6% at 100 µM. The half-maximal concentration (IC_{50}) of the biofilm formation inhibition was calculated as 76.1 µM.

Conidiogenone F (**3**) inhibited *S. aureus* growth by 17.6% when it was used at 100 µM. At 12.5 µM, conidiogenone F (**3**) did not influence *S. aureus* growth. Moreover, conidiogenone F (**3**) prevented *S. aureus* biofilm formation by 10–15% only at concentrations of 50 µM and 100 µM. Leptosphin C; (**4**) inhibited *S. aureus* growth by 42.4% and 10.3% at 100 µM and 12.5 µM, respectively. Moreover, leptosphin C; (**4**) prevented the biofilm formation by 54.5% at 100 µM. The IC_{50} for biofilm formation inhibition was calculated as 85.5 µM.

Antaketide A (5) and tetraketide derivative 6 showed similar inhibition effects on *S. aureus* growth and biofilm formation. Antaketide A (5) inhibited *S. aureus* growth by 48.5% at 100 μM , and this one did not show any influence on *S. aureus* growth at 12.5 μM . Compound 6 inhibited *S. aureus* growth by 46.5% and 25.6% at 100 μM and 12.5 μM , respectively. In addition, 5 and 6 prevented the biofilm formation of *S. aureus* by nearly 30–40%.

The effects of compounds 1–6 on the growth and biofilm formation of Gram-negative bacteria *Escherichia coli* are presented in Figure 9.

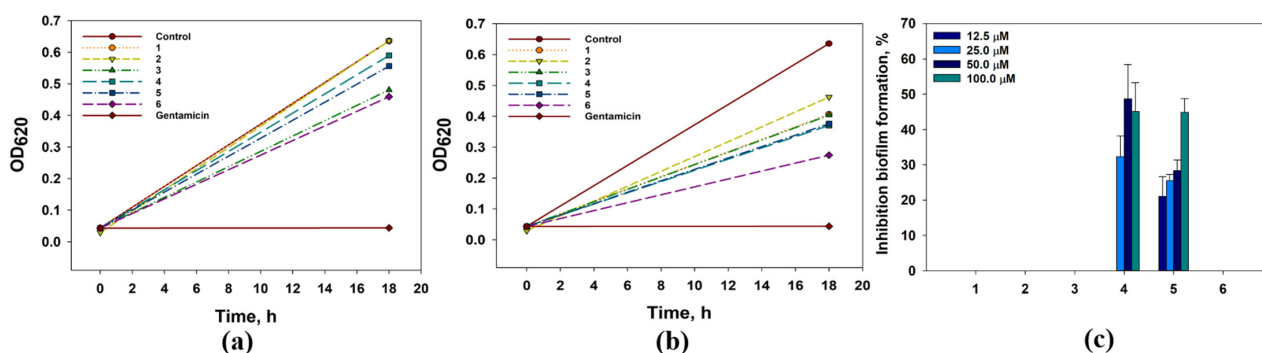


Figure 9. The effect of compounds 1–6 at concentrations of 12.5 μM (a) and 100.0 μM (b) on *E. coli* growth. Gentamicin was used as a positive control at a concentration of 1 mg/mL. (c) The effect of compounds 1–6 on the biofilm formation. The data are presented as a mean \pm standard mean error. All experiments were carried out in independent triplicates.

All investigated compounds inhibited the growth of *E. coli* culture but only compounds 4 and 5 affect the biofilm formation of *E. coli*. 4-Hydroxyleptosphin C (1) and 13-epiconidiogone F (2) at a concentration of 100 μM inhibited *E. coli* growth by 35.9% and 27.3%, respectively. The growth inhibitory effect of these two compounds was not observed when its concentration was 12.5 μM .

Conidiogone F (3) and leptosphin C; (4) at a concentration of 100 μM inhibited *E. coli* growth by 36.4% and 41.7%, respectively. At 12.5 μM , conidiogone F (3) inhibited *E. coli* growth by 24.3% while leptosphin C; (4) inhibited it by only 7.2%. Nevertheless, 4, at concentrations of 25–100 μM , prevented *E. coli* biofilm formation by nearly 30–40%.

Antaketide A (5) at 100 μM and 12.5 μM inhibited *E. coli* growth by 40.9% and 12.5%, respectively. Moreover, 5 prevented the biofilm formation by 21–45% at concentrations of 12.5–100 μM , respectively. Finally, tetraketide derivative 6 at 100 μM and 12.5 μM inhibited *E. coli* growth by 56.9% and 27.7%, respectively, and IC_{50} was calculated as 84.9 μM .

The effects of compounds 1–6 on the growth and biofilm formation of *Candida albicans* are presented in Figure 10.

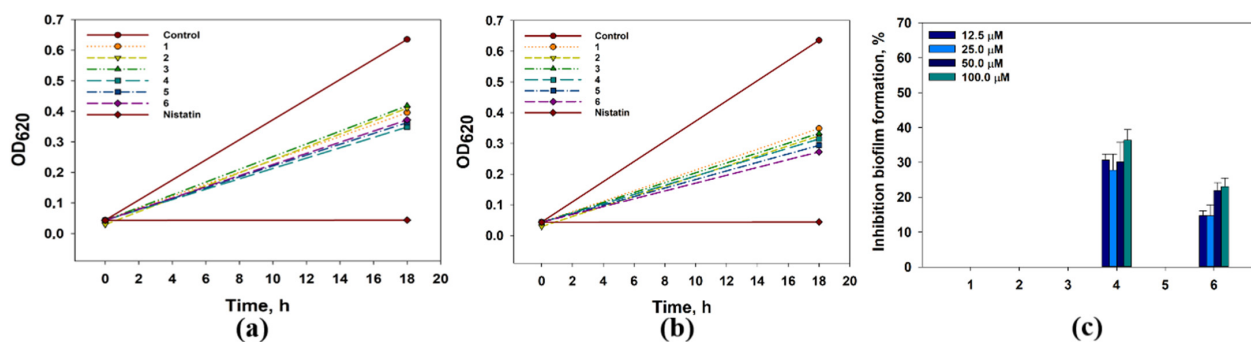


Figure 10. The effect of compounds 1–6 at concentrations of 12.5 μM (a) and 100.0 μM (b) on *C. albicans* growth. The effect of compounds 1–6 on the biofilm formation. Nitrofungin was used as a positive

control at a concentration of 1 mg/mL. The data are presented as a mean \pm standard mean error. All experiments were carried out in independent triplicates.

All compounds inhibited *C. albicans* growth by nearly 30–40%, and compounds 4 and 6 also affected the biofilm formation by *C. albicans*. Compounds 1–3 at a 12.5 μ M inhibited *C. albicans* growth by 30.4%, 27.9%, and 26.5%, respectively. Compound 4 inhibited *C. albicans* growth by 38.7–44.8% and the biofilm formation by 30.6–36.4% at concentrations from 12.5 to 100 μ M. Compound 5 inhibited *C. albicans* growth by 36.2–48.4% and did not affect the biofilm formation. Compound 6 inhibited *C. albicans* growth by 34.7–52.1% and the biofilm formation by 14.7–23.1% at concentrations from 12.5 to 100 μ M. Its IC_{50} for *C. albicans* growth was calculated as 89.9 μ M.

2.3.2. The Influence on Sortase A Activity

Sortase A enzyme is key for biofilm formation and virulence of *S. aureus* and sortase A inhibitors can prevent the biofilm formation [24]. Therefore, a natural inhibitor of sortase A activity rhodionin decreases the adhesion of *S. aureus* to fibrinogen via reducing the capacity of protein A on the bacterial surface and biofilm formation without affecting the survival and growth of bacteria [25].

The investigated compounds 1–6 significantly reduced the formation of *S. aureus* biofilm; therefore, the influence of compounds 1–6 on the activity of sortase A studied in a cell-free test using SensoLyte 520 Sortase A Activity Assay Kit Fluorometric and data are presented in Figure 11.

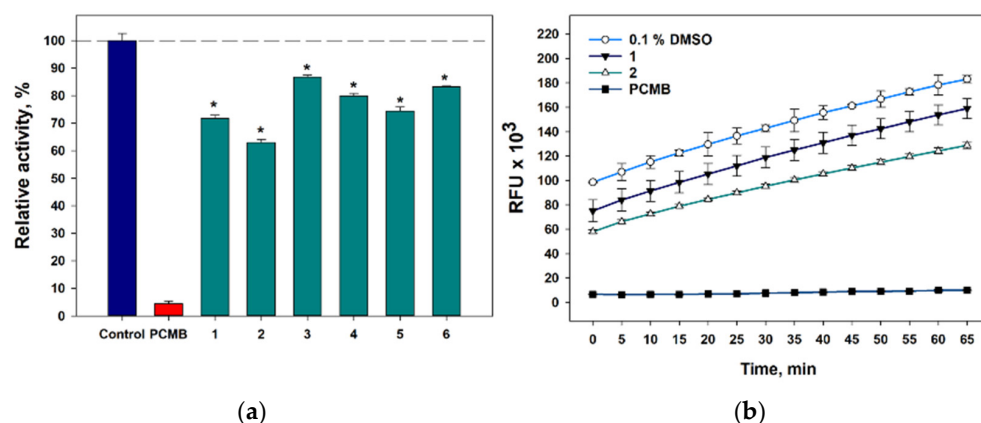


Figure 11. The effects of compounds 1–6 on sortase A activity after 10 min of incubation (a) and time-dependent graph of the inhibitory effect of 4-hydroxyeptosphin C (1) and 13-*epi*-conidiogenone F (2). (b) 4-(Hydroxymercuri)benzoic acid (PCMB) was used as a control. All experiments were carried out in triplicate. The data are presented as a mean \pm standard error of the mean (SEM). * indicates significant differences between the control (DMSO 0.8%) and compounds (p value \leq 0.05).

All compounds at 50 μ M statistically significantly inhibited the activity of sortase A (Figure 11a). 4-Hydroxyeptosphin C (1) and 13-*epi*-conidiogenone F (2) inhibited sortase A activity by 28.2% and 36.9%, and this effect continued during all experiments (Figure 11b). Compounds 3–6 inhibited the sortase A activity by 13.1%, 20.0%, 25.5%, and 16.8%, respectively.

13-*epi*-Conidiogenone F (2) is a stereo isomer of conidiogenone F (3) at C-13, and the β -position of OH-group at C-13 in the structure of 2 is possibly better for interaction with sortase A that caused higher inhibition of sortase A activity. To confirm or refute this assumption as well as determine the contribution of an additional OH-group to the activity of 1, we carried out the molecular docking of compounds 1–4 with sortase A structure (PDB ID 1T2P) using SwissDock [26].

In the apo structure of sortase A (PDB ID 1T2P), a V-shaped pocket is formed by the β 4, β 7, and β 8 strands on one side of the β barrel, together with three surrounding loops. The left side of the pocket is a hydrophobic tunnel formed by Ala92, Ala104, Ala118, Val161, Pro163, Val166, Val 168, Ile182, Val193, Trp194, Ile199, and Val201, along with two putative catalytic residues: Cys184 and Arg197. The right side of the pocket consists of several polar residues: Glu105, Asn114, Ser116, and Thr180 [27].

In our calculations, the most active sortase A inhibitor, 13-*epi*-conidiogenone F (**2**), can form a pose ($\Delta G = -7.16274$ kcal/mol) with the hydrogen-bonding interaction between Glu105 and its OH-group at C-13, and hydrophobic interaction between the keto-group at C1 and Gly192 as well as another hydrophobic interaction with Ala92, Thr93, Thr187, Trp194, and Ala104 (Table 3).

Table 3. The results of molecular docking of compounds 1–4 with sortase A structure (PDB ID 1T2P).

Compound	FF Score, kcal/mol	ΔG , kcal/mol	Hydrogen-Bonding Interactions	Hydrophobic Interactions
1	−3553.963	−7.4239464	Arg197 ... O (at C-4), 2.226 Å	Ala104, Ile182, Ala92, Thr93
	−3549.677	−6.722709	Arg197 ... O2 (at C-13), 2.234 Å OH-group at C-4 ... Glu105, 1.876 Å	Ile199, Ile182,
2	−3531.3604	−6.4623137	Arg197 ... O (at C-1), 2.681 Å OH-group at C-13 ... Glu105, 2.118 Å	Gly192, Val193, Ala104
	−3541.7644	−7.16274	OH-group at C-13 ... Glu105, 2.097 Å	Ala92, Thr93, Thr187, Trp194, Ala104, Gly192
3	−3539.8362	−6.2875967	Arg197 ... OH-group at C-13, 2.668 Å	Ala104, Ile182,
4	−3548.0125	−6.429369	Arg197 ... O (at C-13), 2.493 Å	Ile182
	−3549.6343	−7.032929	no	Ala92, Gly192, Ile182, Ala104

Conidiogenone F (**3**) can form a pose ($\Delta G = -6.2875967$ kcal/mol) with the hydrogen-bonding interaction between Arg197 and its OH-group at C-13 and hydrophobic interactions with only Ala104 and Ile182.

4-Hydroxyleptosphin C (**1**) can form a pose ($\Delta G = -6.722709$ kcal/mol) with the hydrogen-bonding interactions between its keto-group at C-4 and Arg197 and OH-group at C-4 and Glu105 and hydrophobic interactions with Ile199, Ile182. Another stable pose ($\Delta G = -7.4239464$ kcal/mol) formed with the hydrogen-bonding interaction between Arg197 and the keto-group at C-4 and hydrophobic interactions with Ala104, Ile182, Ala92, and Thr93.

Finally, leptosphin C; (**4**) can form a pose ($\Delta G = -6.429369$ kcal/mol) with the hydrogen-bonding interaction between Arg197 and its keto-group at C-13 and hydrophobic interactions with Ile182. Another stable pose ($\Delta G = -7.032929$ kcal/mol) has no hydrogen-bonding interactions and hydrophobic interactions with Ala92, Gly192, Ile182, and Ala104.

Thus, the α -OH-group at C-13 in the structure of **2** allows 13-*epi*-conidiogenone F (**2**) to form the interactions with the amino acid residue of sortase A from both sides of diterpene moiety (Figure 12b). At the time, the β -OH-group at C-13 in the structure of **3** allows for the interaction on only one side of the molecule (Figure 12c). The additional hydroxy group in the structure of **1** also allows this compound to contract with **4** forms the interactions with the amino acid residue of sortase A from both sides of the diterpene moiety (Figure 12a,d).

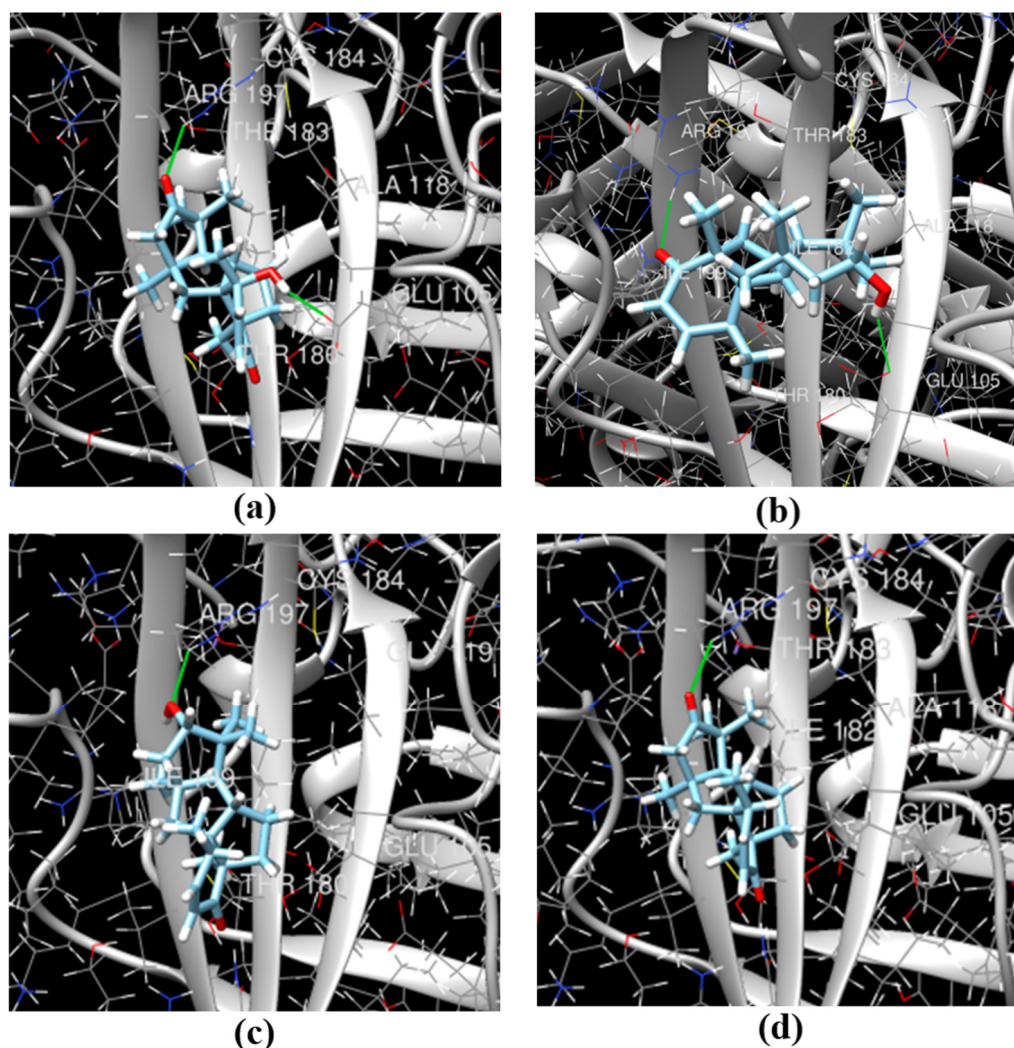


Figure 12. The molecular docking poses of cyclopiane diterpenes 1–4 with sortase A (PDB ID 1T2P): 1 (a), 2 (b), 3 (c), 4 (d).

2.3.3. The Cardiotoxicity of Compounds 1–6

Therefore, secondary metabolites from marine fungus *P. antarcticum* KMM 4670 as inhibitors of *S. aureus* sortase A and the biofilm formation can be promising for future investigations, but its toxicity toward mammalian cells should be tested before such conclusions. Cardiovascular toxicity remains a major cause of concern during preclinical and clinical development, as well as contributing to a post-approval withdrawal of medicines [28]. Therefore, macrolides erythromycin, azithromycin, and clarithromycin cause QT prolongation, torsades de pointes, and arrhythmia-affected cardiomyocyte mitochondria in isolated rat heart mitochondria [29]. The cardiotoxicity of fluoroquinolones was discussed in the review [30]. Thus, the investigation of the cardiotoxicity of leading molecules and drug candidates is actually in the pre-clinical stage. At this time, only three cultivating cardiomyocyte cultures, murine HL-1, rat H9c2, and human AC-16 cell lines, are available. Despite the limitations, the H9c2 cell line is the most used in various experiments [31], including the study of antibiotics' cardiotoxicity [32].

The effect of compounds 1–6 on the viability of H9c2 cardiomyocytes is presented in Table 4.

Table 4. The effect of compounds 1–6 on the viability of H9c2 cardiomyocytes.

Compound	Cell Viability, %		
	1 μ M	10 μ M	100 μ M
1	94.8 \pm 5.9	65.7 \pm 9.4	63.2 \pm 0.5
2	98.1 \pm 1.9	107.3 \pm 7.8	67.3 \pm 3.1
3	103.3 \pm 3.2	92.9 \pm 2.5	109.7 \pm 9.2
4	107.2 \pm 2.9	101.7 \pm 4.6	92.3 \pm 1.9
5	94.4 \pm 3.1	88.5 \pm 3.1	74.1 \pm 4.9
6	98.1 \pm 1.6	80.9 \pm 2.9	54.6 \pm 2.1

Therefore, polyketides **5** and **6** showed significant toxicity toward normal cardiomyocytes at the concentrations in which they affected the growth of microorganisms indicates their non-specific action against living cells.

Both compounds **1** and **2** caused the H9c2 viability to decrease by nearly 30% at a concentration of 100 μ M. Moreover, compound **1** caused the decrease in H9c2 cell viability, near 30%, at a concentration of 10 μ M, while compound **2–4** was non-toxic.

3. Discussion

3.1. Cyclopiane Derivatives from *P. antarcticum* KMM 4670

Cyclopiane-type diterpenes were discovered 20 years ago, and since then, about 25 related compounds have been described. These compounds are usually produced by a number of fungi of the subgenus *Penicillium*, except one report of an isolation from a fungus of the genus *Leptosphaeria*. Structurally, cyclopienes are characterized by a conserved 5/5/5/6 tetracyclic core with methyl groups at C-4, C-9, C-11, and C-14 as well as an oxygenated C-1 atom. The biogenesis of cyclopiane diterpenes was proposed from geranyl geraniol pyrophosphate via hypothetical deoxyconidiogenol [21]. Unfortunately, the absolute stereoconfigurations of these compounds were not established in most of the published works, and in a number of other works, the absolute stereochemistry is questionable. This has led to high confusion about stereostructures of cyclopienes. This study is the very first proof of absolute stereoconfigurations of known conidiogenone F (**3**) and leptosphin C; (**4**) using a modified Mosher's method. Despite the identity of the ECD data of compound **3** with conidiogenone F, the absolute stereostructure of **3** established by us is a mirror structure of that proposed earlier for conidiogenone F [19]. It should be noted that, in recent papers [33,34], conidiogenone F was depicted identically to that established by us. However, no evidence for such an absolute stereostructure has been previously published. The absolute stereostructure of leptosphin C (**4**), determined by us from the obvious biogenetic relationship with conidiogenone F (**3**), is also enantiomeric in comparison with the previously published [21].

Earlier it was reported that conidiogenone F (**3**) at 50 μ g/mL inhibited bacteria *Escherichia coli* growth and did not inhibit the growth of *Staphylococcus aureus* when this one was used at concentrations up to 100 μ g/mL [21]. Our own experiments confirm that conidiogenone F (**3**) is more active against Gram-negative *E. coli* growth.

In the same work, it was reported that leptosphin C (**4**) showed antibacterial activity against *Staphylococcus aureus* (100 μ g/mL) and *Escherichia coli* (>100 μ g/mL) as well as another bacterial strain [21]. In this work, authors used bacterial suspension at a concentration of 10^6 CFU per milliliter and did not use any instrumental equipment for the detection of bacterial growth inhibition. This probably explains why the authors recorded the activity of **3** and **4** at concentrations 166 μ M and 333 μ M (calculated from 50 and 100 μ g/mL) only, whereas in our experiments the activity was detected at significantly lower concentrations.

3.2. Polyketides from *P. antarcticum* KMM 4670

As was shown recently, tetraketide **5** and pentaketide **6** are intermediates in the biosynthesis of cladosporin (**7**). Thus, **6** is formed from a linear tetraketide precursor by its

cyclization, and **5** is the product of the elongation of **6**, with one unit of malonyl-CoA. Both compounds are biosynthesized by the highly reducing I type polyketide synthase. Further formation of cladosporin is controlled by another non-reducing I type polyketide synthase [35]. It proves the absolute stereostructures of both compounds to be the same with cladosporin (**7**). It should be noted that **6** was isolated earlier as a product of the synthetic degradation of cladosporin [36], and its epimer was reported as a civet constituent [22]. Synthetic N-acetylcysteamine thioester derivative of **5** was used for the in vitro biosynthesis of cladosporin by non-reducing I type polyketide synthase [35]. Thus, the current research is the very first report of isolation of cladosporin precursors **5** and **6** as individual natural compounds.

Earlier the antimicrobial activity for **6** was not reported. In our experiments, this one and antaketide A (**5**) showed the highest inhibition activity against the growth of all used test-strains. However, they significantly inhibited biofilm formation in the *S. aureus* culture only, and this effect was supported by the inhibition of sortase A activity. However, we observed the cytotoxicity of the cladosporin precursors **5** and **6** to H9c2 cardiomyocytes, which makes these compounds not as promising leading molecules as we would like.

3.3. Biological Activity of Cyclopiane Diterpenes

Cyclopiane diterpenes **1–4** have a little difference in their chemical structures, but these differences result in differences in their bioactivity. According to their cytotoxic activity, substances can be arranged in the following order: $1 > 2 > 3 = 4$. According to their ability to inhibit the microbial growth, it will be the order: $4 > 1 > 2 = 3$ (*S. aureus*), $3 > 4 > 1 = 2$ (*E. coli*), and $1 = 2 = 3 = 4$ (*C. albicans*), but the differences are not so big. According to their ability to inhibit biofilm formation, it will be the order: $2 = 4 > 1 > 3$ (*S. aureus*), $4 \gg 1 = 2 = 3$ (*E. coli*), and $4 \gg 1 = 2 = 3$ (*C. albicans*). Finally, the order of compounds according to their ability to inhibit the sortase A activity is $2 > 1 > 4 > 3$.

Obviously, that the presence of an additional OH-group at C-4 in the structure of the compound new cyclopiane diterpene 4-hydroxyleptosphin C (**1**), in contrast with leptosphin C (**4**), resulted in its higher cytotoxic and sortase A inhibition activities.

It is believed that antibiotics aimed at the vital functions of bacteria cause the development of resistance much faster. The appearance of penicillin-resistant *S. aureus* strains was registered in 1949, while penicillin was put into practice in the early 40s. The appearance of methicillin and vancomycin-resistant strains was also not long in coming [37]. The identification and analysis of the virulence factors used by pathogens to colonize, invade, and persist within a susceptible host resulted in a new strategy, suggesting that drugs blocking these factors without killing the bacteria create less evolutionary pressure and diminish the chances of resistant genes to emerge. This strategy offers the targeting of the inhibition of the quench pathogen quorum sensing systems or the inhibition of the biofilm formation in the discovery of new antibiotics [38].

Bacteria can survive in two forms: planktonic cells and biofilm, and the formation of biofilm depends on many factors, including the attachment of cell wall components to the cell wall [39]. Staphylococcal sortase A (EC 3.4.22.70) is the cysteine transpeptidase and mainly acts as an anchor surface protein [40]. About 25 years have passed since the beginning of the study of sortase A inhibitors [41], and during this time, a large amount of experimental data has accumulated [42]. Experiments involving laboratory animals confirm that sortase A inhibitors are effective not only in in vitro, but also in in vivo studies [43]. For example, flavonol glycoside hibifolin inhibited sortase A activity, decreased the adhesion of *S. aureus* bacteria to the host cells and the biofilm formation, and, in combination with cefotaxime, protected mice from *S. aureus* infection-induced pneumonia [44].

The natural compounds of various classes, such as alkaloids, polyketides, quinones, and others, were described as sortase A inhibitors. In our experiments, first, it was shown that cyclopiane diterpenes can affect sortase A activity and biofilm formation. The compounds 13-*epi*-conidiogenone F (**2**) and 4-hydroxyleptosphin C (**1**) showed a more effective inhibition of sortase A activity, but 4-hydroxyleptosphin C (**1**) had more cardiotoxicity.

Leptosphin C; (4) inhibited sortase A activity less than 13-*epi*-conidiogenone F (2) but can also be interesting for future investigations due to the low cardiotoxicity.

4. Materials and Methods

4.1. General Experimental Procedures

Optical rotations were measured on a Perkin–Elmer 343 polarimeter (Perkin Elmer, Waltham, MA, USA). UV spectra were recorded on a Shimadzu UV-1601PC spectrometer (Shimadzu Corporation, Kyoto, Japan) in methanol. CD spectra were measured with a Chirascan-Plus CD spectrometer (Leatherhead, UK) in methanol. NMR spectra were recorded in CDCl₃, acetone-*d*₆, and DMSO-*d*₆ on a Bruker DPX-300 (Bruker BioSpin GmbH, Rheinstetten, Germany), a Bruker Avance III-500 (Bruker BioSpin GmbH, Rheinstetten, Germany), and a Bruker Avance III-700 (Bruker BioSpin GmbH, Rheinstetten, Germany) spectrometer, using TMS as an internal standard. HRESIMS spectra were measured on a Maxis impact mass spectrometer (Bruker Daltonics GmbH, Rheinstetten, Germany). Microscopic examination and photography of fungal cultures were performed with Olympus CX41 microscope equipped with an Olympus SC30 digital camera. Detailed examination of ornamentation of the fungal conidia was performed using scanning electron microscopy (SEM) EVO 40.

Low-pressure liquid column chromatography was performed using silica gel (60/100 µm, Imid Ltd., Krasnodar, Russia) and Gel ODS-A (12 nm, S—75 µm, YMC Co., Ishikawa, Japan). Plates precoated with silica gel (5–17 µm, 4.5 cm × 6.0 cm, Imid Ltd., Russia) and silica gel 60 RP-18 F₂₅₄S (20 cm × 20 cm, Merck KGaA, Darmstadt, Germany) were used for thin-layer chromatography. Preparative HPLC was carried out on an Agilent 1100 chromatograph (Agilent Technologies, Santa Clara, CA, USA) with an Agilent 1100 refractometer (Agilent Technologies, Santa Clara, CA, USA) and a Shimadzu LC-20 chromatograph (Shimadzu USA Manufacturing, Canby, OR, USA) with a Shimadzu RID-20A refractometer (Shimadzu Corporation, Kyoto, Japan) using YMC ODS-AM (YMC Co., Ishikawa, Japan) (5 µm, 10 × 250 mm), YMC ODS-AM (YMC Co., Ishikawa, Japan) (5 µm, 4.6 × 250 mm), a HyperClone ODS (Phenomenex, Torrance, CA, USA) (5 µm, 4.6 × 250 mm), and Hydro-RP (Phenomenex, Torrance, CA, USA) (4 µm, 10 × 250 mm) columns.

4.2. Fungal Strain

The fungal strain KMM 4670 was isolated from submarine soil sample collected in the Sea of Okhotsk (the northeastern shelf of the Sakhalin Island). Earlier, the strain KMM 4670 was described by Kirichuk N.N. et al. [3] as a new species “*Penicillium ochotense*” closely related to *Penicillium antarcticum* (section *Canescentia*, series *Atroveneta*) based on DNA sequences of the ITS (internal transcribed spacer), *BenA* (β-tubulin), and *CaM* (calmodulin) regions. During this study, the strain was re-sequenced and re-identified based on sequences of ITS, partial *BenA*, *CaM*, and *RPB2* (RNA polymerase second large subunit) regions. The fungal strain is stored in the Collection of Marine Microorganisms (PIBOC FEB RAS, Vladivostok, Russia) under the code KMM 4670.

4.3. DNA Extraction and Amplification

Genomic DNA was isolated from fungal mycelium grown on MEA (malt extract agar) at 25 °C for 7 days using the MagJET Plant Genomic DNA Kit (Thermo Fisher Scientific, Waltham, MA, USA) according to the manufacturer’s protocol. PCR was conducted using GoTaq Flexi DNA Polymerase (Promega, Madison, WI, USA). For amplification of the ITS gene, the standard primer pair, ITS1 and ITS4 [45], was used. The reaction profile was 95 °C for 300 s; 35 cycles of 95 °C for 20 s, 55 °C for 30 s, 72 °C for 90 s; and, finally, 72 °C for 300 s. For amplification of the partial *BenA* gene, the primer pair, tub_P/A_F (5'-GGTAACCAAATYGGTGCTGCTTTC-3') and Bt-2b [46], was used. The reaction profile was 95 °C for 150 s; 35 cycles of 95 °C for 20 s, 60 °C for 30 s, and 72 °C for 90 s; and, finally, 72 °C for 300 s. For amplification of the partial *CaM* gene, the degenerate primer pair, cal_P/A_F (5'-TCYGAGTACAAGGAGGCSTT-3') and cal_P/A_R (5'-CCRATGGAGGTCATRACGTG-

3'), was used. The reaction profile was 95 °C for 300 s; 35 cycles of 95 °C for 20 s, 65 °C for 30 s, and 72 °C for 90 s; and, finally, 72 °C for 300 s. For amplification of the partial *RPB2* gene, the degenerate primer pair, *rpb2_Pen_F* (5'-GAGACYAAAYCGBGARATYTA-3') and *rpb2_Pen_R* (5'-GTCATSACAATCATRATDGT-3'), was used. The reaction profile was an initial denaturation at 95 °C for 300 s, followed by 5 cycles of 95 °C for 20 s, 48 °C for 30 s, and 72 °C for 90 s; 5 cycles of 95 °C for 20 s, 50 °C for 30 s, and 72 °C for 90 s; 25 cycles of 95 °C for 20 s, 52 °C for 30 s, and 72 °C for 90 s; and, finally, 72 °C for 420 s. The amplified *ITS*, *BenA*, *CaM*, and *RPB2* genes were purified with the ExoSAP-IT™ PCR Product Cleanup Reagent (Thermo Fisher Scientific, Waltham, MA, USA). Sequencing was bidirectionally performed with the same primers on an Applied Biosystems SeqStudio Genetic Analyzer (Thermo Fisher Scientific, Waltham, MA, USA) using the Big Dye Terminator reagent kit, version 3.1. Gene sequences were deposited in GenBank under accession numbers KU358553.2 for *ITS*, KU358556.2 for the partial *BenA*, KU358559.2 for the partial *CaM*, and OR271597 for the partial *RPB2* (Table 1).

4.4. Phylogenetic Analysis

The *ITS* region, the partial *BenA*, *CaM*, and *RPB2* gene sequences of the fungal strain KMM 4670 and other members from the section *Canescentia*, series *Atroveneta*, were aligned using MEGA X software version 11.0.9 [47] using Clustal W algorithm. The ex-type homologs were searched in the GenBank database (<http://ncbi.nlm.nih.gov>, accessed on 8 November 2023) using the BLASTN algorithm (<http://www.ncbi.nlm.nih.gov/BLAST>, accessed on 20 July 2023). The phylogenetic analysis was conducted using MEGA X software [47]. The *ITS* region and partial *BenA*, *CaM*, and *RPB2* gene sequences were concatenated into one alignment. Phylogenetic tree was constructed according to the Maximum Likelihood (ML) algorithm based on the Tamura–Nei model [48]. The tree topology was evaluated with 1000 bootstrap replicates. The *Aspergillus glaucus* NRRL 116^T strain was used in the phylogenetic analysis as outgroup (Table 5).

Table 5. The strains of the species used in multi-locus phylogenetic analysis and GenBank accession numbers.

Species	Strain Number	GenBank Accession Number			
		<i>ITS</i>	<i>BenA</i>	<i>CaM</i>	<i>RPB2</i>
<i>Penicillium atrovenetum</i> G. Smith	CBS 241.56 ^T	AF033492	JX140944	KJ867004	JN121467
<i>Penicillium antarcticum</i> A.D. Hocking & C.F. McRae	CBS 100492 ^T	KJ834503	MN969371	MN969236	JN406653
<i>Penicillium antarcticum</i>	KMM 4670	KU358553	KU358556	KU358559	OR271597
<i>Penicillium coralligerum</i> Nicot and Pionnat	CBS 123.65 ^T	JN617667	MN969378	MN969248	JN406632
<i>Penicillium nucicola</i> Visagie, Malloch, and Seifert	CBS 140987 ^T	KT887860	KT887821	KT887782	MN969171
<i>Penicillium novae-zeelandiae</i> J.F.H. Beyma	CBS 137.41 ^T	JN617688	MN969390	MN969279	JN406628
<i>Aspergillus glaucus</i> Link	NRRL 116 ^T	EF652052	EF651887	EF651989	EF651934

^T—ex-type strain.

4.5. Cultivation of Fungus for Metabolite Isolation

The fungal strain KMM 4670 was cultured on a rice medium at 22 °C for three weeks in 100 Erlenmeyer flasks (500 mL), each containing 20 g of rice, 20 mg of yeast extract, 10 mg of KH₂PO₄, and 40 mL of natural seawater from the Marine Experimental Station of PIBOC, Troitsa (Trinity) Bay, the Sea of Japan.

4.6. Extraction and Isolation

At the end of cultivation, the mycelium of the fungal strain KMM 4670, together with the medium, was homogenized and extracted with EtOAc (1 L). The obtained extract was concentrated in vacuo. The dry residue (57.5 g) was dissolved in H₂O–EtOH (4:1) (300 mL) and extracted successively with *n*-hexane (3 × 0.2 L), EtOAc (3 × 0.2 L), and butanol-1 (3 × 0.2 L). The ethyl acetate extract was evaporated to dryness (2.6 g) and chromatographed on a silica gel column (3 × 14 cm), which was first eluted with *n*-hexane–

EtOAc from 100% *n*-hexane with a stepwise gradient of 10% to 100% EtOAc (total volume 20 L). Fractions of 250 mL were collected and combined based on TLC data.

The fraction eluted with EtOAc–*n*-hexane (20:80, 765 mg) was separated on a YMC ODS-A column (1.5 × 5.5 cm), which was eluted with a step gradient from 40% to 100% MeOH in H₂O (total volume 1 L). Subfraction I, eluted with MeOH–H₂O (40:60, 46 mg), was purified with HPLC on a YMC ODS-AM column (5 μm, 10 × 250 mm), eluted MeOH–H₂O (40:60), and on Phenomenex Hydro-RP column (4 μm, 10 × 250 mm) to give compounds **5** (10.1 min, 4.6 mg) and **6** (9.0 min, 1.2 mg). Subfraction II, eluted with MeOH–H₂O (60:40, 62 mg), was separated on a YMC ODS-AM column, and then, it was re-chromatographed with HPLC on a HyperClone ODS column (5 μm, 4.6 × 250 mm), eluted with MeCN–H₂O (55:45), to give compounds **1** (12.0 min, 0.7 mg), **2** (8.8 min, 0.6 mg), **3** (10.0 min, 2.8 mg), and **4** (14.9 min, 6.7 mg).

4.7. Spectral Data

4-Hydroxyleptosphin C (**1**): $[\alpha]_D^{20}$ —71.43 (c 0.007, MeOH); UV (MeOH) λ_{\max} (log ϵ) 219 (3.78), 198 (3.79), 210 (3.77) (Figure S23 from Supplementary Materials CD (c 2.21 mM, MeOH) λ_{\max} ($\Delta\epsilon$) 196 (−5.13), 208 (−0.15), 238 (−6.17), 300 (0.36), 345 (1.14) nm, (Figure S24 from Supplementary Materials ¹H and ¹³C NMR data are provided in Table 1 (Figures S1 and S2 from Supplementary Materials); HRESIMS m/z 339.1933 [M+Na]⁺ (calcd for C₂₀H₂₈O₃Na 339.1931).

13-*epi*-Conidiogenone F (**2**): $[\alpha]_D^{20}$ —38.30 (c 0.006, MeOH); UV (MeOH) λ_{\max} (log ϵ) 195 (3.86) (Figure S25 from Supplementary Materials CD (c 0.33 mM, MeOH) λ_{\max} ($\Delta\epsilon$) 207 (−1.25), 220 (−1.30), 255 (0.10), 288 (0.03), 3296 (0.06) nm (Figure S26 from Supplementary Materials); ¹H and ¹³C NMR data are provided in Table 1 (Figures S8 and S9 from Supplementary Materials); HRESIMS m/z 325.2142 [M+Na]⁺ (calcd for C₂₀H₃₀O₂Na 325.2138).

Antaketide A (**5**): $[\alpha]_D^{20}$ —108.3 (c 0.012, MeOH), UV (MeOH) λ_{\max} (log ϵ) (Figure S31 from Supplementary Materials); CD (c 0.99 mM, MeOH) λ_{\max} ($\Delta\epsilon$) nm, (Figure S32 from Supplementary Materials ¹H and ¹³C NMR data are provided in Table 2 (Figures S1–S20 from Supplementary Materials); HRESIMS m/z 225.1097 [M+Na]⁺ (calcd for C₁₀H₁₈O₄Na 225.1097).

4.8. Preparation of (S)-MTPA and (R)-MTPA Esters of Conidiogenone F (**3**)

A few crystals of 4-dimethylaminopyridine and (R)-MTPA-Cl (5 μL) were added to a solution of **3** (0.6 mg) in anhydrous pyridine at room temperature and stirred for 4 h. After evaporation of the solvent, the residue was purified with HPLC on a YMC Chiral column (MeCN–H₂O, 90:10) to afford the (S)-MTPA ester (10.8 min, 0.65 mg). The (R)-MTPA ester (11.6 min, 0.16 mg) was prepared in a similar manner using (S)-MTPA-Cl.

(S)-MTPA ester of **3** (**3a**): ¹H NMR (CDCl₃, 500.13 MHz) δ : 6.985 (1H, q, J = 10.1, 5.9 Hz, H-3), 5.973 (1H, dd, J = 10.1, 0.9 Hz, H-2), 5.043 (1H, t, J = 8.7 Hz, H-13), 3.524 (3H, d, J = 0.9 Hz, OMe), 2.692 (1H, m, H-4), 2.304–2.249 (2H, m, H-12, H-6), 2.100 (1H, m, H-8), 2.043 (1H, d, J = 14.6 Hz, H-10), 1.570–1.684 (3H, m, H-12, H-10), 1.309 (3H, s, H-18), 1.252 (3H, brd, J = 7.2 Hz, H-16), 1.166 (3H, s, H-17), 1.018 (3H, s, H-20), 1.006 (3H, s, H-19) (Figure S42 from Supplementary Materials). HRESIMS m/z 541.2541 [M + Na]⁺ (calcd for C₂₉H₃₇O₄F₃Na, 541.253615, Δ = 0.9 ppm) (Figure S44).

(R)-MTPA ester of **1** (**3b**): ¹H NMR (CDCl₃, 500.13 MHz) 6.987 (1H, q, J = 10.1, 5.9 Hz, H-3), 5.977 (1H, dd, J = 10.1, 0.9 Hz, H-2), 5.106 (1H, t, J = 8.7 Hz, H-13), 3.536 (3H, d, J = 0.9 Hz, OMe), 2.697 (1H, m, H-4), 2.267–2.224 (2H, m, H-12, H-6), 2.100 (1H, m, H-8), 2.043 (1H, d, J = 14.6 Hz, H-10), 1.730 (1H, q, J = 14.0, 9.3 Hz, H-12), 1.589–1.691 (2H, m, H-10), 1.349 (3H, s, H-18), 1.259 (3H, brd, J = 7.2 Hz, H-16), 1.168 (3H, s, H-17), 0.964 (3H, s, H-20), 0.915 (3H, s, H-19) (Figure S44 from Supplementary Materials). HRESIMS m/z 541.2542 [M + Na]⁺ (calcd for C₂₉H₃₇O₄F₃Na, 541.253615, Δ = 0.9 ppm) (Figure S41).

4.9. The Quantum Chemical Calculations

The quantum chemical modeling of geometry and spectroscopic properties of compounds **1** and **4** was performed using Gaussian 16 package of programs [49]. Geometry optimizations and calculations IR spectra were performed with B3LYP exchange-correlation functional, the polarization continuum model (PCM), and 6-311G(d) split-valence basis set using default algorithms.

Two important conformations of **1** were found; their statistical weights (g_{im}) were calculated via Gibbs free energies:

$$g_{im} = \frac{e^{-\Delta G_{im}/RT}}{\sum_i e^{-\Delta G_{im}/RT}} \quad (1)$$

where index “*m*” denotes the most stable conformation and $\Delta G_{im} = G_i - G_m$ are the relative Gibbs free energies. The contributions of translational, rotational, vibrational, and electronic motions to G_{im} were calculated at temperature $T = 298.15$ K.

The ECD spectra were calculated using time-dependent density functional theory (TDDFT), cam-B3LYP functional, PCM model, and 6-311G(d) basis set. Twenty-five electronic transitions were calculated for each conformation of **1** and **4**. The individual bands in theoretical spectra were simulated as Gauss-type functions with the bandwidths $\zeta = 0.44$ eV. The UV shifts $\Delta\lambda = 17$ nm and 14 nm were used for best correspondence between experimental and calculated spectra for compounds **1** and **4**, respectively.

4.10. Antimicrobial Activity

The yeast-like fungi of *Candida albicans* KMM 455 and bacterial strains *Staphylococcus aureus* ATCC 21027 and *Escherichia coli* VKPM (B-7935) (Collection of Marine Microorganisms PIBOC FEB RAS) were cultured on solid medium Mueller Hinton broth with agar (16.0 g/L) in a Petri dish at 37 °C for 24 h.

The assays were performed in 96-well microplates in appropriate Mueller Hinton broth. Each well contained 90 μ L of bacterial or of yeast-like fungi suspension (10^9 CFU/mL). Then, 10 μ L of a compound diluted at concentrations from 1.5 μ M to 100.0 μ M using two-fold dilution were added (DMSO concentration <1%). Culture plates were incubated for 18 h at 37 °C, and the OD₆₂₀ was measured using a Multiskan FS spectrophotometer (Thermo Scientific Inc., Beverly, MA, USA). The antibiotic gentamicin and the antifungal agent nitrofungin were used as positive controls at 1 mg/mL; 1% DMSO in PBS served as a negative control [50].

4.11. Biofilm Formation Assay

The inhibition reducing biofilm formation and growth was assessed using the crystal violet biofilm assay as described [24]. Overnight cultures of bacteria *S. aureus* and *E. coli* and yeast-like fungi *C. albicans* were inoculated into Mueller–Hinton broth at a concentration of 10^9 CFU/mL. A total of 90 μ L of this cell suspension was then dispensed into 96-well microtiter plates containing 10 μ L of different concentrations of compounds **1–6**. After 24 h growth at 37 °C, the plates were washed with PBS to remove unbound cells. Next, the wells were stained with 0.1% crystal violet solution for 10 min at 37 °C. At the completion of the incubation, plates were washed 3 times with PBS and dried. Then, the crystal violet dye from the biofilm was solubilized with 100 μ L of ethanol. A total of 100 μ L of this solution was then moved to a new microtiter plate for absorbance measurement at $\lambda = 570$ nm. The results were reported as percent inhibition normalized to the wild-type control.

4.12. Sortase A Activity Inhibition Assay

The enzymatic activity of sortase A from *S. aureus* was determined using SensoLyte 520 Sortase A Activity Assay Kit Fluorimetric (AnaSpec AS-72229, AnaSpec, San Jose, CA, USA) in accordance with the manufacturer’s instructions. The compounds were dissolved in DMSO and diluted with reaction buffer to obtain a final concentration of 0.8% DMSO,

which did not affect enzyme activity. DMSO at a concentration of 0.8% was used as a control. 4-(Hydroxymercuri)benzoic acid (PCMB) was used as sortase A enzyme activity inhibitor. Fluorescence was measured with a plate reader PHERAStar FS (BMG Labtech, Offenburg, Germany) for 60 min, with a time interval of 5 min. The data were processed with MARS Data Analysis v. 3.01R2 (BMG Labtech, Offenburg, Germany). The results were presented as relative fluorescent units (RFUs) and percentage of the control data, calculated using STATISTICA 10.0 software.

4.13. Cell Culture

The rat cardiomyocytes H9c2 cells were kindly provided by Prof. Dr. Gunhild von Amsberg from Martini-Klinik Prostate Cancer Center, University Hospital Hamburg-Eppendorf, Hamburg, Germany.

The H9c2 cells were cultured in DMEM medium (Biolot, St. Petersburg, Russia) containing 10% fetal bovine serum (Biolot, St. Petersburg, Russia) and 1% penicillin/streptomycin (Biolot, St. Petersburg, Russia) at 37 °C in a humidified atmosphere with 5% (*v/v*) CO₂.

4.14. Cell Viability Assay

The H9c2 cells were seeded at concentrations of 3×10^3 cell/well, and the experiments were started after 24 h. The compounds at concentrations up to 100 µM were added into the wells for 24 h, and the viability of the cells was measured with an MTT (3-(4,5-dimethylthiazol-2-yl)-2,5-diphenyltetrazolium bromide) assay, which was performed according to the manufacturer's instructions (Sigma-Aldrich, Munich, Germany). All compounds were dissolved with DMSO so that the final concentration of DMSO in the cell culture was not more than 1%. Moreover, DMSO was used as a control. The results were presented as a percent of the control data and calculated IC₅₀.

4.15. Molecular Docking

The pdb file of sortase A (PDB ID 1T2P) was obtained from the RCSB Protein Data Bank (<https://www.rcsb.org>, accessed on 8 November 2023) and prepared for docking with the PrepDock package of UCFS Chimera 1.16 software. The chemical structures of ligands were prepared for docking with ChemOffice and checked with the PrepDock package of UCFS Chimera 1.16 software.

Docking was conducted on the SwissDock online server (<http://www.swissdock.ch>, accessed on 8 November 2023) based on EADock DSS docking software [51]. The algorithm implies the generation of many binding modes in the vicinity of all target cavities (blind docking) and estimation of their CHARMM energies via the Chemistry at HARvard Macromolecular Mechanics (CHARMM) algorithm [52] for evaluation of the binding modes with the most favorable energies with FACTS (Fast Analytical Continuum Treatment of Solvation) [53] and, finally, clustering of these binding modes [54].

The predicted building models for each target/ligand pair were visualized and analyzed with UCFS Chimera 1.16 software. Docking parameters, such as Gibb's free energy (ΔG , kcal/mol), FullFitness score (FF, kcal/mol), and hydrogen-bonding and hydrophobic interactions, were used for analysis of target/ligand complexes.

4.16. Statistical Data Evaluation

All data were obtained in three independent replicates, and calculated values were expressed as a mean \pm standard error mean (SEM). Student's *t*-test was performed using SigmaPlot 14.0 (Systat Software Inc., San Jose, CA, USA) to determine statistical significance. Differences were considered statistically significant at $p < 0.05$.

5. Conclusions

Two new cyclopiane diterpenes and a new cladosporin precursor, together with four known related compounds, were isolated from marine sediment-derived fungus *P. antarcticum* KMM 4670. The absolute stereostructures of conidiogenone F and leptosphin

C were determined for the first time. This study is the very first report of the isolation of cladospurin precursors **5** and **6** as individual natural compounds. New cyclopiane diterpene 13-*epi*-conidiogenone F (**2**) is very promising for future investigation as an anti-staphylococcal agent.

Supplementary Materials: The following supporting information can be downloaded at: <https://www.mdpi.com/article/10.3390/md21110584/s1>, Figures S1–S27: NMR spectra of compounds **1–6**; Figures S38–S43: MS spectrum of compounds **1–6**; Figures S28, S30, S32, S34, S36: UV spectra of compounds **1–5**; Figures S29, S31, S33, S35, S37: CD spectra of compounds **1–5**; Figures S44–S45, S47–S48: NMR spectra of compounds **3a** and **3b**; Figures S46, S49: MS spectrum of compounds **3a** and **3b**.

Author Contributions: Conceptualization, O.I.Z. and E.A.Y.; Data curation, A.N.Y.; Formal analysis, A.N.Y., N.N.K. and E.A.Y.; Investigation, O.I.Z., O.O.K., G.K.O., A.S.A., N.N.K., V.E.C., A.I.K., D.V.B., N.Y.K., R.S.P., E.A.C., A.R.C. and E.A.Y.; Methodology, M.P.I.; Project administration, M.P.I.; Resources, A.N.Y. and M.P.I.; Software, D.V.B. and M.P.I.; Supervision, A.N.Y. and M.P.I.; Validation, A.N.Y., O.I.Z., V.E.C., M.P.I. and E.A.Y.; Visualization, O.O.K., N.N.K., V.E.C., D.V.B., E.A.C. and E.A.Y.; Writing—original draft, A.N.Y., N.N.K., V.E.C. and D.V.B.; Writing—review & editing, M.P.I. and E.A.Y. All authors have read and agreed to the published version of the manuscript.

Funding: This study was funded by a grant from the Ministry of Science and Higher Education of Russian Federation 15.BRK.21.0004 (Contract No. 075-15-2021-1052).

Institutional Review Board Statement: Not applicable.

Data Availability Statement: The original data presented in the study are included in the article/Supplementary Materials; further inquiries can be directed to the corresponding author.

Acknowledgments: The study was carried out using the Collective Facilities Center “Collection of Marine Microorganisms PIBOC FEB RAS” and on the equipment of the Collective Facilities Center, “The Far Eastern Center for Structural Molecular Research (NMR/MS) PIBOC FEB RAS”.

Conflicts of Interest: The authors declare no conflict of interest. The funders had no role in the design of the study; in the collection, analyses, or interpretation of data; in the writing of the manuscript; or in the decision to publish the results.

References

1. Wang, C.; Tang, S.; Cao, S. Antimicrobial compounds from marine fungi. *Phytochem. Rev.* **2021**, *20*, 85–117. [[CrossRef](#)]
2. Yurchenko, A.N.; Girich, E.V.; Yurchenko, E.A. Metabolites of Marine Sediment-Derived Fungi: Actual Trends of Biological Activity Studies. *Mar. Drugs* **2021**, *19*, 88. [[CrossRef](#)] [[PubMed](#)]
3. Kirichuk, N.N.; Pivkin, M.V.; Matveeva, T.V. Three new *Penicillium* species from marine subaqueous soils. *Mycol. Prog.* **2017**, *16*, 15–26. [[CrossRef](#)]
4. Visagie, C.M.; Frisvad, J.C.; Houbraeken, J.; Visagie, A.; Samson, R.A.; Jacobs, K. A re-evaluation of *Penicillium* section *Canescentia*, including the description of five new species. *Persoonia Mol. Phylogeny Evol. Fungi* **2021**, *46*, 163–187. [[CrossRef](#)] [[PubMed](#)]
5. Marchese, P.; Mahajan, N.; O’Connell, E.; Fearnhead, H.; Tuohy, M.; Krawczyk, J.; Thomas, O.P.; Barry, F.; Murphy, M.J. A novel high-throughput screening platform identifies itaconate derivatives from marine *Penicillium antarcticum* as inhibitors of mesenchymal stem cell differentiation. *Mar. Drugs* **2020**, *18*, 192. [[CrossRef](#)]
6. Vansteelandt, M.; Kerzaon, I.; Blanchet, E.; Tankoua, O.F.; Du Pont, T.R.; Joubert, Y.; Monteau, F.; Le Bizec, B.; Frisvad, J.C.; Pouchus, Y.F. Patulin and secondary metabolite production by marine-derived *Penicillium* strains. *Fungal Biol.* **2012**, *116*, 954–961. [[CrossRef](#)]
7. Geiger, M.; Guitton, Y.; Vansteelandt, M.; Kerzaon, I.; Blanchet, E.; Robiou du Pont, T.; Frisvad, J.C.; Hess, P.; Pouchus, Y.; Grovel, O. Cytotoxicity and mycotoxin production of shellfish-derived *Penicillium* spp., a risk for shellfish consumers. *Lett. Appl. Microbiol.* **2013**, *57*, 385–392. [[CrossRef](#)] [[PubMed](#)]
8. Leshchenko, E.V.; Antonov, A.S.; Borkunov, G.V.; Hauschild, J.; Zhuravleva, O.I.; Khudyakova, Y.V.; Menshov, A.S.; Popov, R.S.; Kim, N.Y.; Graefen, M. New Bioactive β -Resorcylic Acid Derivatives from the Alga-Derived Fungus *Penicillium antarcticum* KMM 4685. *Mar. Drugs* **2023**, *21*, 178. [[CrossRef](#)]
9. Shiono, Y.; Seino, Y.; Koseki, T.; Murayama, T.; Kimura, K.-i. Antarones A and B, two polyketides from an endophytic *Penicillium antarcticum*. *Z. Naturforschung B* **2008**, *63*, 909–914. [[CrossRef](#)]
10. Leshchenko, E.V.; Antonov, A.S.; Dyshlovoy, S.A.; Berdyshev, D.V.; Hauschild, J.; Zhuravleva, O.I.; Borkunov, G.V.; Menshov, A.S.; Kirichuk, N.N.; Popov, R.S.; et al. Meroantarctines A-C, Meroterpenoids with Rearranged Skeletons from the Alga-Derived

- Fungus *Penicillium antarcticum* KMM 4685 with Potent p-Glycoprotein Inhibitory Activity. *J. Nat. Prod.* **2022**, *85*, 2746–2752. [[CrossRef](#)]
11. Afiyatullo, S.S.; Zhuravleva, O.I.; Antonov, A.S.; Leshchenko, E.V.; Pivkin, M.V.; Khudyakova, Y.V.; Denisenko, V.A.; Pislyagin, E.A.; Kim, N.Y.; Berdyshev, D.V.; et al. Piltunines A–F from the Marine-Derived Fungus *Penicillium piltunense* KMM 4668. *Mar. Drugs* **2019**, *17*, 647. [[CrossRef](#)] [[PubMed](#)]
 12. Scott, P.M.; Van Walbeek, W.; MacLean, W.M. Cladosporin, a new antifungal metabolite from *Cladosporium cladosporioides*. *J. Antibiot.* **1971**, *24*, 747–755. [[CrossRef](#)] [[PubMed](#)]
 13. Hoepfner, D.; McNamara, C.W.; Lim, C.S.; Studer, C.; Riedl, R.; Aust, T.; McCormack, S.L.; Plouffe, D.M.; Meister, S.; Schuierer, S. Selective and specific inhibition of the *Plasmodium falciparum* lysyl-tRNA synthetase by the fungal secondary metabolite cladosporin. *Cell Host Microbe* **2012**, *11*, 654–663. [[CrossRef](#)]
 14. Pang, L.; Weeks, S.D.; Van Aerschot, A. Aminoacyl-tRNA Synthetases as Valuable Targets for Antimicrobial Drug Discovery. *Int. J. Mol. Sci.* **2021**, *22*, 1750. [[CrossRef](#)] [[PubMed](#)]
 15. Anke, H.; Zähner, H.; König, W.A. Metabolic products of microorganisms. *Arch. Microbiol.* **1978**, *116*, 253–257. [[CrossRef](#)] [[PubMed](#)]
 16. Wang, X.; Wedge, D.E.; Cutler, S.J. Chemical and Biological Study of Cladosporin, an Antimicrobial Inhibitor: A Review. *Nat. Prod. Commun.* **2016**, *11*, 1595–1600. [[CrossRef](#)]
 17. Hou, A.; Li, B.; Deng, Z.; Xu, M.; Dickschat, J.S. Cladosporin, A Highly Potent Antimalaria Drug? *ChemBioChem* **2023**, *24*, e202300154. [[CrossRef](#)] [[PubMed](#)]
 18. Baragaña, B.; Forte, B.; Choi, R.; Nakazawa Hewitt, S.; Bueren-Calabuig, J.A.; Pisco, J.P.; Peet, C.; Dranow, D.M.; Robinson, D.A.; Jansen, C. Lysyl-tRNA synthetase as a drug target in malaria and cryptosporidiosis. *Proc. Natl. Acad. Sci. USA* **2019**, *116*, 7015–7020. [[CrossRef](#)]
 19. Du, L.; Li, D.; Zhu, T.; Cai, S.; Wang, F.; Xiao, X.; Gu, Q. New alkaloids and diterpenes from a deep ocean sediment derived fungus *Penicillium* sp. *Tetrahedron* **2009**, *65*, 1033–1039. [[CrossRef](#)]
 20. Gao, S.S.; Li, X.M.; Zhang, Y.; Li, C.S.; Wang, B.G. Conidiogenones H and I, two new diterpenes of cyclopiane class from a marine-derived endophytic fungus *Penicillium chrysogenum* QEN-24S. *Chem. Biodivers.* **2011**, *8*, 1748–1753. [[CrossRef](#)]
 21. Chen, H.Y.; Liu, T.K.; Shi, Q.; Yang, X.L. Sesquiterpenoids and diterpenes with antimicrobial activity from *Leptosphaeria* sp. XL026, an endophytic fungus in *Panax notoginseng*. *Fitoterapia* **2019**, *137*, 104243. [[CrossRef](#)]
 22. Maurer, B.; Grieder, A.; Thommen, W. (cis-6-Methyltetrahydropyran-2-yl)acetic acid, a novel compound from civet (*Viverra civetta*). *Helv. Chim. Acta* **1979**, *62*, 44. [[CrossRef](#)]
 23. Kusumi, T.; Ooi, T.; Ohkubo, Y.; Yabuuchi, T. The modified Mosher's method and the sulfoximine method. *Bull. Chem. Soc. Jpn.* **2006**, *79*, 965–980. [[CrossRef](#)]
 24. Thappeta, K.R.; Zhao, L.N.; Nge, C.E.; Crasta, S.; Leong, C.Y.; Ng, V.; Kanagasundaram, Y.; Fan, H.; Ng, S.B. *In-Silico* Identified New Natural Sortase A Inhibitors Disrupt *S. aureus* Biofilm Formation. *Int. J. Mol. Sci.* **2020**, *21*, 8601. [[CrossRef](#)] [[PubMed](#)]
 25. Wang, X.; Luan, Y.; Hou, J.; Jiang, T.; Zhao, Y.; Song, W.; Wang, L.; Kong, X.; Guan, J.; Song, D.; et al. The protection effect of rhodionin against methicillin-resistant *Staphylococcus aureus*-induced pneumonia through sortase A inhibition. *World J. Microbiol. Biotechnol.* **2022**, *39*, 18. [[CrossRef](#)] [[PubMed](#)]
 26. Daina, A.; Michielin, O.; Zoete, V. SwissTargetPrediction: Updated data and new features for efficient prediction of protein targets of small molecules. *Nucleic Acids Res.* **2019**, *47*, W357–W364. [[CrossRef](#)] [[PubMed](#)]
 27. Zong, Y.; Bice, T.W.; Ton-That, H.; Schneewind, O.; Narayana, S.V.L. Crystal Structures of *Staphylococcus aureus* Sortase A and Its Substrate Complex. *J. Biol. Chem.* **2004**, *279*, 31383–31389. [[CrossRef](#)] [[PubMed](#)]
 28. Ferri, N.; Siegl, P.; Corsini, A.; Herrmann, J.; Lerman, A.; Benghozi, R. Drug attrition during pre-clinical and clinical development: Understanding and managing drug-induced cardiotoxicity. *Pharmacol. Ther.* **2013**, *138*, 470–484. [[CrossRef](#)]
 29. Salimi, A.; Eybagi, S.; Seydi, E.; Naserzadeh, P.; Kazerouni, N.P.; Pourahmad, J. Toxicity of macrolide antibiotics on isolated heart mitochondria: A justification for their cardiotoxic adverse effect. *Xenobiotica* **2016**, *46*, 82–93. [[CrossRef](#)]
 30. Rubinstein, E.; Camm, J. Cardiotoxicity of fluoroquinolones. *J. Antimicrob. Chemother.* **2002**, *49*, 593–596. [[CrossRef](#)]
 31. Onódi, Z.; Visnovitz, T.; Kiss, B.; Hambalkó, S.; Koncz, A.; Ágg, B.; Váradi, B.; Tóth, V.É.; Nagy, R.N.; Gergely, T.G.; et al. Systematic transcriptomic and phenotypic characterization of human and murine cardiac myocyte cell lines and primary cardiomyocytes reveals serious limitations and low resemblances to adult cardiac phenotype. *J. Mol. Cell. Cardiol.* **2022**, *165*, 19–30. [[CrossRef](#)] [[PubMed](#)]
 32. Hajimirzaei, N.; Khalili, N.P.; Boroumand, B.; Safari, F.; Pourhosseini, A.; Judi-Chelan, R.; Tavakoli, F. Comparative Study of the Effect of Macrolide Antibiotics Erythromycin, Clarithromycin, and Azithromycin on the ERG1 Gene Expression in H9c2 Cardiomyoblast Cells. *Drug Res.* **2020**, *70*, 341–347. [[CrossRef](#)] [[PubMed](#)]
 33. Li, F.; Sun, W.; Zhang, S.; Gao, W.; Lin, S.; Yang, B.; Chai, C.; Li, H.; Wang, J.; Hu, Z.; et al. New cyclopiane diterpenes with anti-inflammatory activity from the sea sediment-derived fungus *Penicillium* sp. TJ403-2. *Chin. Chem. Lett.* **2020**, *31*, 197–201. [[CrossRef](#)]
 34. Zhang, S.; He, Y.; Li, F.; Lin, S.; Yang, B.; Mo, S.; Li, H.; Wang, J.; Qi, C.; Hu, Z.; et al. Bioassay-directed Isolation of antibacterial metabolites from an arthropod-derived *Penicillium chrysogenum*. *J. Nat. Prod.* **2020**, *83*, 3397–3403. [[CrossRef](#)] [[PubMed](#)]

35. Cochrane, R.V.K.; Sanichar, R.; Lambkin, G.R.; Reiz, B.; Xu, W.; Tang, Y.; Vederas, J.C. Production of New Cladosporin Analogues by Reconstitution of the Polyketide Synthases Responsible for the Biosynthesis of this Antimalarial Agent. *Angew. Chem. Int. Ed.* **2016**, *55*, 664–668. [[CrossRef](#)] [[PubMed](#)]
36. Rawlings, B.J.; Reese, P.B.; Ramer, S.E.; Vederas, J.C. Comparison of fatty acid and polyketide biosynthesis: Stereochemistry of cladosporin and oleic acid formation in *Cladosporium cladosporioides*. *J. Am. Chem. Soc.* **1989**, *111*, 3382. [[CrossRef](#)]
37. de Oliveira Santos, J.V.; da Costa Júnior, S.D.; de Fátima Ramos dos Santos Medeiros, S.M.; Cavalcanti, I.D.L.; de Souza, J.B.; Coriolano, D.L.; da Silva, W.R.C.; Alves, M.H.M.E.; Cavalcanti, I.M.F. Panorama of Bacterial Infections Caused by Epidemic Resistant Strains. *Curr. Microbiol.* **2022**, *79*, 175. [[CrossRef](#)]
38. Mahdally, N.H.; George, R.F.; Kashaf, M.T.; Al-Ghobashy, M.; Murad, F.E.; Attia, A.S. Staquorsin: A Novel Staphylococcus aureus Agr-Mediated Quorum Sensing Inhibitor Impairing Virulence in vivo without Notable Resistance Development. *Front. Microbiol.* **2021**, *12*, 700494. [[CrossRef](#)]
39. Nitulescu, G.; Margina, D.; Zanfirescu, A.; Olaru, O.T.; Nitulescu, G.M. Targeting bacterial sortases in search of anti-virulence therapies with low risk of resistance development. *Pharmaceuticals* **2021**, *14*, 415. [[CrossRef](#)]
40. Kudryavtsev, K.V.; Fedotcheva, T.A.; Shimanovsky, N.L. Inhibitors of Sortases of Gram-Positive Bacteria and their Role in the Treatment of Infectious Diseases (Review). *Pharm. Chem. J.* **2021**, *55*, 751–756. [[CrossRef](#)]
41. Ton-That, H.; Schneewind, O. Anchor structure of staphylococcal surface proteins: IV. Inhibitors of the cell wall sorting reaction. *J. Biol. Chem.* **1999**, *274*, 24316–24320. [[CrossRef](#)]
42. Pecoraro, C.; Carbone, D.; Parrino, B.; Cascioferro, S.; Diana, P. Recent Developments in the Inhibition of Bacterial Adhesion as Promising Anti-Virulence Strategy. *Int. J. Mol. Sci.* **2023**, *24*, 4872. [[CrossRef](#)] [[PubMed](#)]
43. Wang, X.; Wei, L.; Wang, L.; Chen, X.; Kong, X.; Luan, Y.; Guan, J.; Guo, X.; Shi, Y.; Wang, T.; et al. Scutellarin potentiates vancomycin against lethal pneumonia caused by methicillin-resistant Staphylococcus aureus through dual inhibition of sortase A and caseinolytic peptidase P. *Biochem. Pharmacol.* **2022**, *199*, 114982. [[CrossRef](#)] [[PubMed](#)]
44. Song, W.; Wang, L.; Zhao, Y.; Lanzi, G.; Wang, X.; Zhang, C.; Guan, J.; Wang, W.; Guo, X.; Meng, Y.; et al. Hibifolin, a Natural Sortase A Inhibitor, Attenuates the Pathogenicity of Staphylococcus aureus and Enhances the Antibacterial Activity of Cefotaxime. *Microbiol. Spectr.* **2022**, *10*, e00950-22. [[CrossRef](#)] [[PubMed](#)]
45. White, T.J.; Bruns, T.; Lee, S.; Taylor, J.W. Amplification and direct sequencing of fungal ribosomal RNA genes for phylogenetics. In *PCR Protocols: A Guide to Methods and Applications*; Innis, M.A., Gelfand, D.H., Sninsky, J.J., White, T.J., Eds.; Academic Press: London, UK, 1990; pp. 315–322.
46. Glass, N.L.; Donaldson, G.C. Development of primer sets designed for use with the PCR to amplify conserved genes from filamentous ascomycetes. *Appl. Environ. Microbiol.* **1995**, *61*, 1323–1330. [[CrossRef](#)] [[PubMed](#)]
47. Kumar, S.; Stecher, G.; Li, M.; Niyaz, C.; Tamura, K. MEGA X: Molecular evolutionary genetics analysis across computing platforms. *Mol. Biol. Evol.* **2018**, *35*, 1547. [[CrossRef](#)] [[PubMed](#)]
48. Tamura, K.; Nei, M. Estimation of the number of nucleotide substitutions in the control region of mitochondrial DNA in humans and chimpanzees. *Mol. Biol. Evol.* **1993**, *10*, 512–526.
49. Frisch, M.J.; Trucks, G.W.; Schlegel, H.B.; Scuseria, G.E.; Robb, M.A.; Cheeseman, J.R.; Scalmani, G.; Barone, V.; Petersson, G.A.; Nakatsuji, H.; et al. *Gaussian 16 Rev. A.03*; Gaussian: Wallingford, CT, USA, 2016.
50. Campbell, J. High-throughput assessment of bacterial growth inhibition by optical density measurements. *Curr. Protoc. Chem. Biol.* **2010**, *2*, 195–208. [[CrossRef](#)]
51. Grosdidier, A.; Zoete, V.; Michielin, O. SwissDock, a protein-small molecule docking web service based on EADock DSS. *Nucleic Acids Res.* **2011**, *39*, W270–W277. [[CrossRef](#)]
52. Brooks, B.R.; Brooks, C.L., III; Mackerell, A.D., Jr.; Nilsson, L.; Petrella, R.J.; Roux, B.; Won, Y.; Archontis, G.; Bartels, C.; Boresch, S.; et al. CHARMM: The biomolecular simulation program. *J. Comput. Chem.* **2009**, *30*, 1545–1614. [[CrossRef](#)]
53. Haberthür, U.; Caflisch, A. FACTS: Fast analytical continuum treatment of solvation. *J. Comput. Chem.* **2008**, *29*, 701–715. [[CrossRef](#)]
54. Grosdidier, A.; Zoete, V.; Michielin, O. Fast docking using the CHARMM force field with EADock DSS. *J. Comput. Chem.* **2011**, *32*, 2149–2159. [[CrossRef](#)]

Disclaimer/Publisher's Note: The statements, opinions and data contained in all publications are solely those of the individual author(s) and contributor(s) and not of MDPI and/or the editor(s). MDPI and/or the editor(s) disclaim responsibility for any injury to people or property resulting from any ideas, methods, instructions or products referred to in the content.